Quantum Simulations of Ne_n-OH^+ Clusters

Markus Meuwly[†]

Department of Chemistry, University of Durham, South Road, Durham, DH1 3LE England

Received: April 11, 2000

Structures and dynamics of Ne_n-OH^+ clusters are investigated using both adiabatically corrected $Ne-OH^+$ dimer potential energy surfaces and a three-dimensional interaction potential. The first rigorous test of the previously developed vibrational adiabatic approximation to construct potential energy surfaces for clusters comprising vibrationally excited monomers against calculations encompassing all coordinates is presented. Good agreement between the different approaches and with experiment is found. Frequency shifts, $\Delta\nu(n)$, for the OH^+ stretching excitation as a function of the number, n, of neon atoms are presented. Under the assumption that the shift for the first completely filled solvation ring is representative an infrared transition of OH^+ in a neon matrix at around 2845 cm^{-1} is predicted. This value includes many-body contributions inferred from recent studies on $Ne_n-HN_2^+$.

1. Introduction

With the advent of sophisticated experimental techniques detailed investigations of small molecular clusters have become possible.[1,2] These studies provide useful information about intermolecular interactions, structures, and energetics of the systems. As a paradigm for stepwise solvation, small aggregates studied under high-resolution constitute an important class of systems for which controlled experiments are possible.[3−5]

This development opens possibilities to address questions of real chemical and biochemical relevance such as the influence of a solvent on the thermodynamics and dynamics of enzymes[6] or effects on reaction rates modified by solvent dynamics.[7]

In this regard the studies performed on charged species have been particularly fruitful.[4,8−11] Usually the clusters consist of an infrared chromophore that is surrounded by structureless atoms or small molecules. In cases where it is possible to follow specific characteristics as a function of the number of solvent moieties around the infrared chromophore, stepwise solvation effects can be investigated.

Some of the systems are small enough to allow accurate theoretical work. This is necessary to devise and test approximate methods. For this purpose, several methodologies have been developed.[12−14] One of the concepts—the adiabatic correction of a potential energy surface—has been specifically designed to include the effect of the monomer vibration into the interaction potential.[15] However, this approach has not yet been tested against fully dimensional calculations. It is one of the aims of the present work to assess the usefulness of the decoupling approach.

For this, the $Ne-OH^+$ ionic complex constitutes an appropriate system. The adiabatically corrected surfaces for the ground and first vibrationally excited state of OH^+ have been constructed and shown to yield satisfactory agreement with experiment.[16] Ab initio calculations of the three-dimensional interaction potential are possible and the ro-vibrational problem can be accurately solved.

In addition, $Ne-OH^+$ is a good candidate for further experiments on microsolvation of ionic chromophores. To this end the vibrational red shift of the OH^+ frequency as a function of the number of neon atoms surrounding the ion is calculated. The three-dimensional potential is used to calculate minimum energy structures and quantum mechanical ground state energies of Ne_n-OH^+ clusters for $n \leq 6$.

This work is structured as follows. In the next section the previously calculated, two-dimensional potential energy surface is extended to include the OH^+ coordinate. Then, the fundamentals on the three-dimensional surface are calculated and compared with results on the adiabatically corrected potential $V_0(R,\theta)$ and $V_1(R,\theta)$. The third part is devoted to the investigation of complexation induced red shifts, structures, and energetics of the Ne_n-OH^+ clusters.

2. Interaction Potential

The present work uses a standard Jacobi coordinate system in which r is the OH distance, R is the distance from the center of mass of OH^+, and θ is the angle between the two distance vectors. It is advantageous to choose the grid on which energies are calculated such as to minimize the effort in subsequent bound state calculations. Evaluation of the necessary angular integrals is most stable if Gauss−Legendre points are used. In addition, the representation of the interaction potential is simplified. Thus, calculations at angles corresponding to an 8-point quadrature ($\theta = 16.20°$, 37.19°, 58.31°, 79.44°, 100.58°, 121.71°, 142.82°, and 163.80°) were performed. The OH^+ bond lengths were $r = 1.76a_0$, $1.948a_0$, and $2.17a_0$; $r = 1.948a_0$ is the optimized OH^+ bond length and the two other points correspond to the inner and outer turning point of the $\nu = 0$ state of the free monomer. The grid of Jacobi radii R included 16 points between $3.8a_0$ and $18a_0$. It should be noted that the Gauss−Legendre grid in θ is different from the equidistant one used previously. In particular, the smaller angles, around which the fundamental excitations are concentrated, are more densely covered.

All ab initio calculations were carried out with the Gaussian 94 suite of programs.[17] Electronic structure calculations at the QCISD(T) level of theory employed the previously used Ahlrichs valence triple-ζ basis set augmented by diffuse and polarization functions from Dunning's aug-cc-pVTZ contrac-

[†] Present address: Departement für Chemie und Biochemie, Universität Bern, Freiestrasse 3, CH-3000 Bern 9, Switzerland.

10.1021/jp001380d CCC: $19.00
Published on Web 07/06/2000

tion.[18,19] As proposed by Boys and Bernardi, the interaction energies were counterpoise corrected.[20]

To verify the suitability of QCISD(*T*) an additional one-dimensional cut through the potential was calculated at the CCSD(*T*) level of theory. Here, $r = 1.948a_0$ and $\theta = 0$ were chosen. The results differ by less than 5 cm^{-1} over the entire range of *R* values.

The interaction in the $Ne-OH^+$ complex is described by

$$E(R,r,\theta) = V(R,r,\theta) + V_{OH^+}(r) \quad (1)$$

where $V_{OH^+}(r)$ is the potential curve for isolated OH^+ and $V(R,r,\theta)$ is the counterpoise corrected potential energy surface for the complex. The OH^+ potential curve has been calculated using the same basis set and correlation treatment as those for the $Ne-OH^+$ complex. To be useful in subsequent bound state calculations, the discrete energy points have to be represented as a continuous function. It is convenient to represent the interaction potential $V(R,r,\theta)$ as an expansion in Legendre polynomials and radial strength functions

$$V(R,r,\theta) = \sum_\lambda V_\lambda(R,r)\, P_\lambda(\theta) \quad (2)$$

Projecting the coefficients $V_\lambda(R,r)$ is most stable if the interaction potential is given at Gauss−Legendre points in θ. The radial strength functions are subsequently represented using a reproducing kernel (RKHS).[21] (A code to construct the interaction potential is available from the author upon request.) Cuts through $V(R,r,\theta)$ for the $r = 1.76a_0$ and $r = 2.17a_0$ are displayed in Figure 1.

The global minimum of the interaction between Ne and OH^+ is found at $r = 1.980a_0$, $R = 5.013a_0$, and $\theta = 0$ and has a well depth of 1251.6 cm^{-1}.

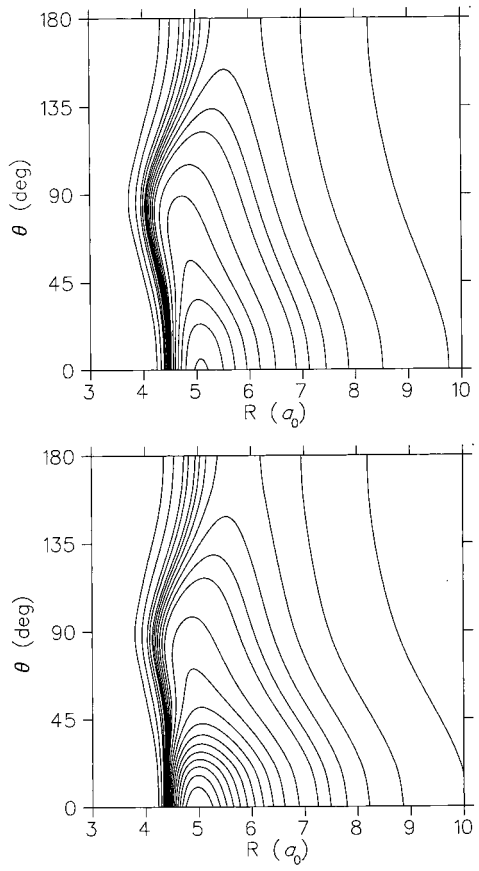

Figure 1. Contour plot of the $Ne-OH^+$ potential energy surface $V(R,r,\theta)$ from QCISD(*T*) calculations for $r = 1.76a_0$ (above) and $2.17a_0$ (below). Between the lowest contour (−800 cm^{-1} for $r = 1.76a_0$ and −1300 cm^{-1} for $r = 2.17a_0$) and −400 cm^{-1} the spacing is 100 cm^{-1}; above it is 50 cm^{-1}. Contours on the repulsive wall are drawn at 100, 200, 500, and 1000 cm^{-1}.

3. Bound State Calculations

In the following the three-dimensional bound state problem for $Ne-OH^+$ is considered. This gives the opportunity to directly assess the validity of the vibrational adiabatic correction.[15] To allow a fair comparison, the bound state calculations on the two adiabatically corrected potentials $V_0(R,\theta)$ and $V_1(R,\theta)$ have to be repeated because the angular grid previously used for the ab initio calculations was different. The form and parameters of the correction function are the ones reported earlier.[19]

Bound state close-coupling calculations are carried out using BOUND.[22] After expanding the total wave function in a product of angular and radial functions, the resulting coupled equations in *R* are solved numerically using a log-derivative propagator.[23,24] All calculations are performed in space-fixed representation.

The reduced mass of the complex is $9.189189m_u$. The coupled equations are propagated from $R_{min} = 2.0$ to $R_{max} = 15.0$ Å and extrapolated to zero step-size from log-derivative interval sizes of 0.02 and 0.04 Å using Richardson h^4 extrapolation.

The nomenclature for the quantum numbers involved is identical to the one used earlier.[16,19] Thus, a state is described by $(v_1 v_b^{lp} v_s)$ where v_1 gives the number of quanta in the OH^+ bond, v_b^{lp} labels the bending together with the parity *p* of the state, and v_s is the stretching coordinate.

To characterize the fundamentals in a useful way, rotational B_v and D_v constants are calculated from a fit of energy levels $E_v(J)$ to a standard diatomic Hamiltonian

$$E_v(J) = E_v + B_v[J(J+1) - K^2] - D_v[J(J+1) - K^2]^2 \quad (3)$$

Here, *K* is the projection of the OH^+ angular momentum *j* on the intermolecular axis.

A. Two-Dimensional Calculations. For the two-dimensional calculations on the adiabatically corrected potentials, the rotational constants for OH^+ were $b_0 = 16.422\,86$ cm^{-1} and $b_1 = 15.695\,26$ cm^{-1}.[25] Monomer rotational levels up to $j = 25$ were included in the basis set, which converges energies to better than 10^{-4} cm^{-1}.

A general observation is that all bound states are found deeper in the well than the previous calculations.[19] This is probably due to the finer grid in θ on which the present ab initio calculations have been carried out. The overall effect is about 10 cm^{-1} for all states. However, shifts in the *relative* energies are considerably smaller. As an example, the stretching vibration $(0\,0^0\,1)$ is found at 154.1 cm^{-1} instead of 151.2 cm^{-1}.

These results are not too surprising as with the present potentials the low-angle region, to which the fundamentals are most sensitive, is better covered. In addition, the spline interpolation previously used overestimated the angular curvature in the potential because only information about the potential at $\theta = 0$ and 30° was available.[19]

B. Three-Dimensional Calculations. Three-dimensional close-coupling calculations require means to evaluate matrix elements between monomer vibrational wave functions. Here, the quadrature scheme proposed by Schwenke and Truhlar is adopted.[26] The three distances *r* on which ab initio calculations for $Ne-OH^+$ were performed are chosen as quadrature points. Anharmonic OH^+ wave functions required to calculate the

TABLE 1: Relative Energies (in cm^{-1}) and Rotational *B* and *D* Constants (in cm^{-1}) of the Fundamentals of Ne−OH$^+$ [a]

	(0 0^0 0)	(0 0^0 1)	(0 1^{1e} 0)	(0 1^{1f} 0)	(0 2^0 0)
exp. (ref 16)					
B	0.25648				
$D/10^{-6}$	2.24				
2-d		154.4	247.4	247.4	290.6
B	0.2516	0.2401	0.2507	0.2515	0.2284
$D/10^{-6}$	2.5	2.9	3.4	3.3	3.8
3-d		158.1	253.8	253.8	297.6
B	0.2517	0.2403	0.2505	0.2513	0.2285
$D/10^{-6}$	2.4	2.8	3.2	3.2	3.6
	(1 0^0 0)	(1 0^0 1)	(1 1^{1e} 0)	(1 1^{1f} 0)	(1 2^0 0)
exp. (ref 16)	2786.5		327	327	
B	0.26044				
$D/10^{-6}$	1.71				
2-d	2792.0	173.1	322.3	322.3	328.1
B	0.2592	0.2482	0.2552	0.2558	0.2366
$D/10^{-6}$	2.2	2.5	2.9	2.9	2.8
3-d	2800.8	178.5	319.0	319.0	337.2
B	0.2566	0.2456	0.2534	0.2540	0.2340
$D/10^{-6}$	2.0	2.3	2.6	2.6	2.7

[a] Energies are given with respect to the ground state of Ne−OH$^+$ (υ_1) except for (1 0^0 0), which is given with respect to (0 0^0 0); the labeling ($\upsilon_1 \upsilon_b^{lp} \upsilon_s$) is the one employed for semirigid triatomics.

integration weights are computed using the LEVEL program.[27] Points and weights constructed in this manner evaluate constant, linear, and quadratic potential terms over *r* exactly. To carry out three-dimensional bound state calculations, monomer ro-vibrational basis functions (υ_1,*j*) have to be specified. They included states up to $\upsilon_1 = 2$ and $j = 11$. The energies of these states are calculated by solving the one-dimensional Schrödinger equation with the QCISD(*T*) potential *V*(*r*) using LEVEL.[27] Convergence studies including higher (υ_1,*j*) basis functions changed the energies by less than 10^{-4} cm^{-1}.

The ground state (0 0^0 0) of Ne−OH$^+$ is found at −839 cm^{-1} below dissociation to Ne + OH$^+$. This amounts to a zero point energy of roughly 400 cm^{-1}. Calculations on $V_0(R,\theta)$ yield a slightly smaller dissociation energy also because the well depth is reduced by 35 cm^{-1}. First stretching (1 0^0 1) and bending (0 $1^{1e/f}$ 0) excitations lie 158 and 254 cm^{-1} higher in energy, which compares to 154 and 247 cm^{-1} on $V_0(R,\theta)$, respectively.

For $\upsilon_1 = 0$ the only rotational constants available from experiment are those for the ground state. The values resulting from calculations on the adiabatically corrected surface underestimate *B* and overestimate *D*. Once the three-dimensional calculation is performed, the values of *B* and *D* change slightly and move in the appropriate direction. Additional comparison between quantities calculated on $V_0(R,\theta)$ and $V(R,r,\theta)$ is given in Table 1.

One possibility to assess approximate ro-vibrational energies for levels correlating with $\upsilon_1 = 1$ is to perform bound state calculations including $\upsilon_1 \geq 1$ monomer basis functions only. Although this might seem to be a drastic procedure, mixing between the $\upsilon_1 = 0$ and $\upsilon_1 = 1$ states can be expected to be small. In second-order perturbation theory matrix elements between $\upsilon_1 = 0$ and $\upsilon_1 = 1$ are of the order of 1 cm^{-1}. More accurate procedures involve the determination of scattering resonances and fitting them to a Breit−Wigner form.[28,29]

The lowest state, correlating with (1 0^0 0), is calculated at 1961 cm^{-1} above the ground state. This gives an energy difference of 2800 cm^{-1} between Ne−OH$^+$ ($\upsilon_1 = 1$) and Ne−OH$^+$ ($\upsilon_1 = 0$). The experimentally measured value is 2786.5 cm^{-1}. Consequently, the vibrational red shift is underestimated by 13.5 cm^{-1}. Excitation of the intermolecular stretch (1 0^0 1) is found 179 cm^{-1} higher followed by the Π (1 1^1 0) (319 cm^{-1}) bending vibration. The experimental value for the Π bending frequency is 327 cm^{-1} whereas a calculation on the adiabatically corrected potential $V_1(R,\theta)$ yields 322 cm^{-1}.

Given the considerably reduced computational effort to construct $V_0(R,\theta)$ and $V_1(R,\theta)$ compared to $V(R,r,\theta)$, the results justify an approximate treatment of the intramolecular degree of freedom *r*. This is even more so as no truly spectroscopically accurate interaction potential can be expected from a pure ab initio calculation. Under these circumstances $V_0(R,\theta)$ and $V_1(R,\theta)$ constitute a useful working hypothesis and a good starting point for further refinement together with future experimental data in the spirit of ref 30.

4. Ne$_n$−OH$^+$ Clusters

In the previous section the reliability of the vibrational adiabatic approximation has been established. Consequently, further explorations of Ne$_n$−OH$^+$ clusters based on the $V_0(R,\theta)$ and $V_1(R,\theta)$ potential energy surfaces can be undertaken. Of immediate interest to experiment is the complexation induced red shift of the OH$^+$ frequency, $\Delta\upsilon(n)$, as a function of the number of neon atoms, *n*. Furthermore, the three-dimensional interaction potential allows one to investigate structural and dynamic characteristics including all coordinates involved.

In the following the interaction between Ne$_n$−OH$^+$ is assumed to be pairwise additive. The Ne−Ne interaction has been thoroughly investigated by Aziz and co-workers.[31] Thus, the total intermolecular potential in a Ne$_n$−OH$^+$ cluster is then given by

$$V_{\mathrm{tot}}(n) = \sum_{i=1}^{n} V_{\mathrm{Ne}_i-\mathrm{OH}^+}(R_i,r,\theta_i) + \sum_{i<j}^{n} V_{\mathrm{Ne-Ne}}(s_{ij}) \qquad (4)$$

Here, *s* is the distance between two neon atoms and *R* and θ describe the usual Jacobi coordinates of the *i*th neon atom with respect to OH$^+$. The indices *i* and *j* run over all Ne atoms in the cluster.

A. Structures of Larger Clusters. Further explorations of Ne$_n$−OH$^+$ clusters may be undertaken using the interaction potential $V(R,r,\theta)$, which depends explicitly upon *r*. The primary interest in this section concerns the dynamics of the clusters, especially the question of how much of the potential energy surface is sampled by clusters of different sizes. However, prior to this it is instructive to consider the minimum energy configurations.

Minimum energy configurations are calculated using the downhill simplex method.[32] Initial configurations to start the minimization are not too difficult to guess because the intermolecular interaction is strongly oriented along the intermolecular bond. In addition, the configuration found for Ne$_{n-1}$−OH$^+$ can be used as the starting configuration for an optimization of Ne$_n$−OH$^+$.

It is of some interest to report minimum energy configurations for several cluster sizes. For $n = 3$, 6, and 12 they are displayed in Figure 2. The terminal neon atom always occupies a strongly linearly oriented position ($\theta = 0$) and the next neon atoms form solvation rings. This is in slight contrast to the recently investigated Ne$_n$−HN$_2^+$ clusters where for Ne$_3$−HN$_2^+$ a configuration without a terminal neon atom was lowest in energy.[33] Otherwise, the solvation rings are filled in a similar manner. The first and second solvation rings contain five neon atoms and the first solvation shell is completed when OH$^+$ is surrounded by 12 neon atoms. Because of the smaller ionic core,

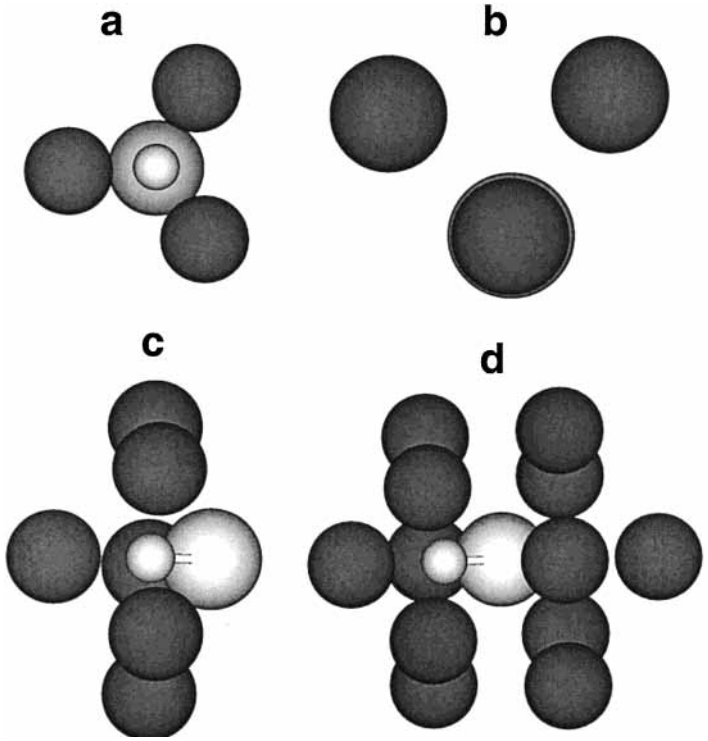

Figure 2. Minimum energy configurations for (a) $Ne_3-HN_2^+$, (b) Ne_3-OH^+, (c) Ne_6-OH^+, and (d) $Ne_{12}-OH^+$. Clearly visible are the different arrangements of the three neon atoms for HN_2^+ (a) or OH^+ (b) as the chromophore. (Dark spheres symbolize neon atoms and the light ones constitute the ionic core.)

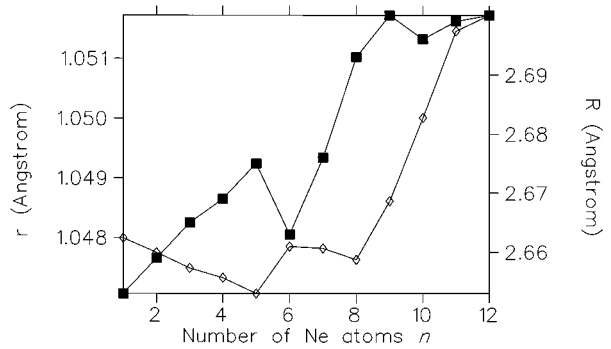

Figure 3. Variation of r (open diamonds) and R (filled squares) for optimized conformations of Ne_n-OH^+ as a function of the number of neon atoms n.

only two instead of three solvation rings as in $Ne_n-HN_2^+$ can be accommodated. As shown in Figure 2, the first and second solvation ring are twisted with respect to each other by 36°. This leads to a very regular arrangement of the neon atoms. However, it should be noted that with less than completely filled solvation rings appreciable distortions occur in which the terminal neon atom leaves the linear configuration.

It should be noted that the reported configurations are not really "structures" of the complexes. These systems are greatly influenced by zero point contributions and will sample wider parts of the interaction potentials than anticipated from pictures as given in Figure 2.

Another point worthwhile mentioning is the response of the OH^+ bond length r as the number n of solvent atoms increases. The graphical representation in Figure 3 shows that r decreases monotonically for $n \leq 5$ before elongation is observed. The slight contraction from 1.048 to 1.047 Å for $n \leq 5$ can be rationalized in a diminished influence of the terminal, collinear neon atom. In going from the $Ne-OH^+$ dimer up to the pentamer, subsequent neon atoms seem to "push" the terminal one away. This is also displayed in Figure 3 where the distance R of the terminal neon atom as a function of n is plotted. At $n = 6$ both r and R change abruptly because there the cluster is in a highly symmetric conformation and the terminal neon atom can occupy its preferred position.

It is of some interest to compare the structures for Ne_n-OH^+ with the experimentally and theoretically studied neutral system Ar_n-HF.[34-36] For the trimer, the argon atoms are arranged in a regular triangle (C_{3v}) whereas for Ne_3-OH^+ the symmetry is only C_s (Figure 2b). The tetramers have identical topologies. In the case of the pentamer, the HF diatom is not clearly immersed in the cluster as for Ne_5-OH^+. The argon atoms seem to form a subcluster to which the diatom is attached to.[36]

These structural differences are a result of the different intermolecular interactions. The well depths for Ar−HF and Ar−Ar are only different by a factor of about 2 whereas for $Ne-OH^+$ and Ne−Ne this ratio is almost 20.

B. Diffusion Monte Carlo Calculations. Clusters containing relatively weakly interacting moieties are subject to appreciable zero point effects. In addition, the strongly anharmonic interaction potentials prevent the use of methods taking only the curvature around the minimum into account. One of the methods that allows to include terms neglected in harmonic approximations is Diffusion Monte Carlo (DMC). DMC is a valuable method to calculate ground state properties for many body systems at zero temperature. A detailed account of DMC for vibrational problems in molecular physics has been given by Suhm and Watts.[37]

Here, the DMC code by V. Buch has been used.[38] To perform a DMC calculation, one has to specify the number of replicas. They are represented by a collection of Gaussian functions centered around an atom or the center of gravity of a subunit and a given width. With these replicas a random walk is performed. For very long simulation times their distribution in space approaches the ground state distribution and accordingly

TABLE 2: Total Energies (in cm^{-1}), E_{tot}, and Ground State Energies Calculated on $V_0(R,\theta)$ and $V(R,r,\theta)$ for Ne_n-OH^+ ($n \leq 6$)

	$Ne-OH^+$	Ne_2-OH^+	Ne_3-OH^+	Ne_4-OH^+	Ne_5-OH^+	Ne_6-OH^+
E_{tot}	−1252	−1819	−2418	−3012	−3612	−4166
E^{2d}_{DMC}	−822 ± 1	−1364 ± 1	−1921 ± 1	−2409 ± 2	−2891 ± 3	−3334 ± 3
E^{3d}_{DMC}	−828 ± 12	−1373 ± 12	−1920 ± 15	−2401 ± 20		

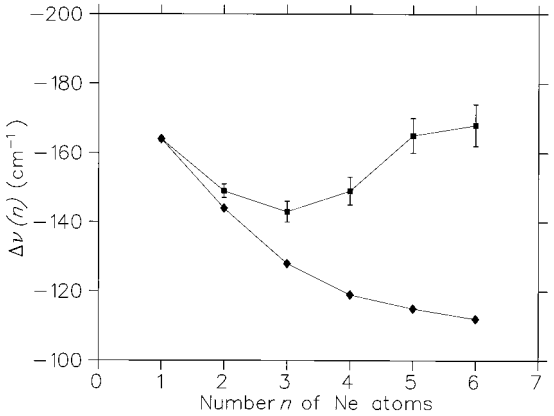

Figure 4. Vibrational red shift of the OH^+ frequency as a function of the number of surrounding neon atoms, *n*. The squares are the bare DMC results with their associated errors; the diamonds represent results that include many-body contributions similar to those of $Ne_n-HN_2^+$.

the quantum mechanical ground state energy. Technically, this is the reference energy that is required to keep the number of replicas stable. Other parameters to be chosen include an equilibration time and a time during which the results are averaged.

The number of replicas was 2500 in all calculations. In each DMC run the first 500 time steps were performed with $\Delta\tau$ = 60 au. For another 500 time steps $\Delta\tau$ was decreased to 30 au during which the 6 simultaneously propagated generations were equilibrated. A total of 20 runs with changing initial conditions was performed and the results were averaged over 3000 time steps. One advantage of DMC is that the initial guess for the wave function does not need to be particularly good. DMC will converge to the correct ground state of the system if the initial distribution of replicas is able to access the relevant regions of the potential and the simulation time is long enough.

C. Complexation Induced Red Shifts $\Delta\nu(n)$. In these DMC calculations the OH^+ monomer bond length is kept frozen at the distance corresponding to the rotational constant for $\upsilon_1 = 0$ (r = 1.0404 Å) and $\upsilon_1 = 1$ (r = 1.0642 Å). Close-coupled calculations for the $Ne-OH^+$ dimer present an accurate target to gauge DMC values. The DMC runs yield −822.4 ± 0.5 and −984.8 ± 1.0 cm^{-1} for the ground states (0 0^0 0) and (1 0^0 0) compared to −822.32 and −985.54 cm^{-1} from close-coupling calculations, respectively. This good agreement makes conclusions drawn from calculations of larger clusters more trustworthy.

Red shifts as a function of the cluster size *n* can be calculated as the difference in stabilization energy between $Ne_n-OH^+(\upsilon = 0)$ and $Ne_n-OH^+(\upsilon = 1)$. These quantities correspond to the total ground state energy of Ne_n-OH^+ clusters calculated on the two adiabatically corrected potentials $V_0(R,\theta)$ and $V_1(R,\theta)$. Red shifts have been calculated for $n \leq 6$ and are shown in Figure 4. As for $Ne_n-HN_2^+$, $\Delta\nu(n)$ first decreases but increases once $n \geq 4$.[33]

Analogous to all previously investigated, protonated ions surrounded by rare gas atoms, it seems reasonable to assume that $\Delta\nu(n)$ is in reality a monotonically decreasing function, at least for the first solvation ring.[4,10,11,39] Thus, it is conceivable that an important ingredient in the present analysis is missing. However, at this point the assumption of pairwise additive interactions might become too serious of an approximation.

Given the similar interaction strength and overall topology of the intermolecular potential, it seems appropriate to use the insight gained in the analysis of $Ne_n-HN_2^+$. There it was found that a repulsive many-body contribution of 5 cm^{-1}/neon pair brings theory and experiment into good agreement. This value is also plausible from direct ab initio calculations of the three-body contribution.[33] It seems justified to apply a similar reasoning to Ne_n-OH^+. In Figure 4 the curve for $\Delta\nu(n)$ including this distance and angle-independent many-body contribution is displayed as well. As can be seen, it approaches a value of ≈110 cm^{-1} for large *n*. For the $Ne-OH^+$ dimer the calculated red-shift underestimates the experimental value by 6 cm^{-1}.[16] Consequently, the reported theoretical red shifts are best considered to be lower bounds to the true values.

As for the structures, it is also interesting to contrast the present observations with the energetics and dynamics of Ar_n-HF clusters. On the basis of high-quality potential energy surfaces for $Ar-HF(\upsilon = 0)$ and $Ar-HF(\upsilon = 1)$ by Hutson (ref 40) DMC[41] and 5D bound state calculations[42] have been performed for various cluster sizes. The vibrational red shifts between 10 and 40 cm^{-1} for the neutral systems are considerably smaller than the ones for $Ne-OH^+$. In contrast to the observation for ionic complexes, the red shifts *increase* with increasing cluster size in the case of Ar_n-HF.[42]

D. Calculations Involving All Degrees of Freedom. Calculations on the fully dimensional potential energy surface involve the motion of the hydrogen atom in a steep potential. Therefore, the DMC parameters had to be changed. To get reasonably converged total energies, shorter time steps and longer simulation times were employed. Sufficiently converged energies are only given for clusters up to $n = 4$ as the simulations get very time consuming. Calculations have been performed for simulation times of 32 000 au with $\Delta\tau$ = 4, 8, and 16 au. The resulting energies and associated statistical errors were extrapolated to zero step size. Table 2 shows that the statistical errors are larger compared to the calculations on the adiabatically corrected potentials. This is mainly due to the fact that now the motion of the hydrogen atom in a rather steep potential is taken into account as well. The average energy for the dimer is −828 ± 12 cm^{-1} compared to −839 cm^{-1} from the close-coupling calculations.

Although neon is a relatively heavy binding partner, zero point effects contribute appreciably to the total energy. For comparison, ground state energies on the adiabatically corrected potential $V_0(R,\theta)$ are given as well in Table 2.

Distribution functions for the quantum mechanical ground state can help to gain further insight into the dynamics of the clusters. To this end, results of the order of 5×10^6 configurations have been averaged.

Projections of configurations of the neon atoms around the ion are displayed in Figure 5. The configurations have been weighted according to their probability in every DMC run and are projected onto a plane containing one neon atom and OH^+. As the number of neon atoms is increased, wider portions of the interaction potential are sampled. A marked increase in the configuration space accessed is observed between $n = 2$ and

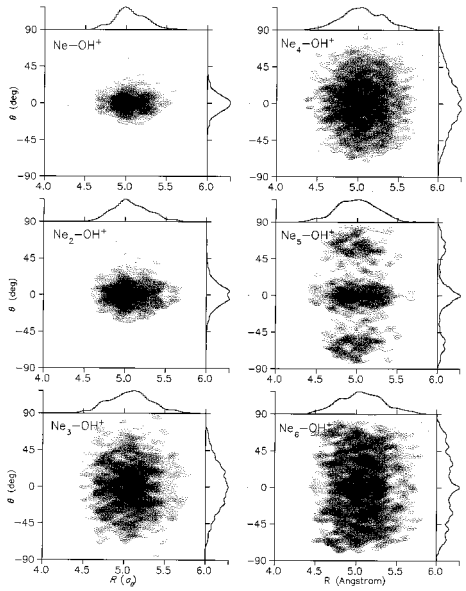

Figure 5. Distribution functions for the neon atoms in $Ne-OH^+$ up to Ne_6-OH^+. The center of mass of OH^+ is in the origin of the coordinate system (not shown). Projections onto the R and θ axes are cumulative probabilities individually normalized to unity.

$n = 3$. This is probably connected with the fact that the configuration where three neon atoms form an equilateral triangle around the hydrogen end is nearly as favorable as the minimum energy configuration that has a terminal neon atom along the intermolecular axis and two neon atoms in the first solvation ring. As a result, the angular distribution function for $n = 3$ is considerably flattened out compared to the one for $n = 2$.

A noteworthy change occurs for $n = 5$. Instead of a smooth, angular distribution function, clearly separated maxima appear. To eliminate the possibility of undersampling, additional DMC calculations with different initial conditions were run. However, the results were always—more or less pronounced—the same. One possible explanation is the formation of a distinct solvation ring that makes an angle of $\theta \approx 70°$ with respect to OH^+. In addition, the trend to spread in R, which can be observed from $n = 1$ to $n = 4$ is not continued. The distribution function seems to be more tightly confined in the radial coordinate.

Finally, for $n = 6$ this "shell" is not apparent at all. Apart from a slight maximum in the linear configuration, an almost uniform distribution over a wide range of θ dominates. The small variations in the angular part of the distribution function are most probably due to undersampling, although additional calculations have been performed like those for $n = 5$.

5. Concluding Remarks

The construction of the adiabatically corrected potentials presented in ref 19 relies on the decoupling of inter- and intramolecular degrees of freedom. Depending on the interaction strength between the ion and the binding partner, this decoupling is more or less complete. However, only a three-dimensional calculation can assess as to which degree and whether this adiabatic separation is appropriate.

The present work has aimed at investigating this point by performing close-coupling calculations on a three-dimensional potential energy surface calculated at the QCISD(T) level of theory. The results show that $V_0(R,\theta)$ and $V_1(R,\theta)$ are useful to describe spectroscopic quantities such as intermolecular excitations, rotational constants, and vibrational red shifts. The vibrational adiabatic correction is an easily applicable procedure, helps to include effects of intermolecular excitations on the same level of theory the potential energy surface is calculated at, and reduces the number of ab initio points required considerably. In addition, these surfaces can be used in further refinement stages together with experimental data.[30,33]

One of the main observables in mid-infrared and matrix isolation studies of neutral and charged van der Waals complexes is the vibrational red shift, $\Delta\nu(n)$. It is a sensitive measure for the interaction of a chromophore with its environment. For Ne_n-OH^+ such measurements are not yet available but might be possible. Estimates for $\Delta\nu(n)$ assuming a pairwise additive interaction in the DMC calculations and a many-body correction of 5 cm^{-1}/neon pair inferred from recent work on $Ne_n-HN_2^+$ are given. A comparison with previously studied microclusters shows that the value at which $\Delta\nu(n)$ flattens out is representative for the red shift that can be expected in a rare gas matrix.[4,10,11,39,43] Thus, OH^+ in a neon matrix is predicted to absorb at a wavelength of about 2845 cm^{-1}.

Conformations and dynamics of Ne_n-OH^+ clusters were investigated using the three-dimensional interaction potential. Diffusion Monte Carlo calculations were performed to include zero point effects. The distribution functions for the neon atoms from such quantum simulations demonstrate that the configuration space sampled by the rare gas atoms is larger than structural optimizations make one believe, even for such relatively strongly interacting systems.

Acknowledgment. The author acknowledges financial support from the Schweizerischer Nationalfonds zur Förderung der wissenschaftlichen Forschung. The calculations were carried out on a Silicon Graphics Origin 2000 computer system, which was purchased with funding from the Engineering and Physical Sciences Research Council. The author thanks both referees for careful reading and constructive criticism of the manuscript.

References and Notes

(1) Greenblatt, B. J.; Zanni, M. T.; Neumark, D. M. *Science* **1997**, *276*, 1675.
(2) Fellers, R. S.; Leforestier, C.; Braly, L. B.; Brown, M. G.; Saykally, R. J. *Science* **1999**, *284*, 945.
(3) Anderson, D. T.; Davis, S.; Nesbitt, D. J. *J. Chem. Phys.* **1997**, *107*, 1115.
(4) Nizkorodov, S. A.; Dopfer, O.; Ruchti, T.; Meuwly, M.; Maier, J. P.; Bieske, E. J. *J. Phys. Chem.* **1995**, *99*, 17118.
(5) Carney, J. R.; Hagemeister, F. C.; Zwier, T. S. *J. Chem. Phys.* **1998**, *108*, 3379.
(6) Brooks, C. L., III; Karplus, M.; Pettitt, B. M. *Adv. Chem. Phys.* **1988**, *71*, 1.
(7) Marcus, R. A. *Adv. Chem. Phys.* **1997**, *101*, 391.
(8) Price, J. M.; Crofton, M. W.; Lee, Y. T. *J. Chem. Phys.* **1989**, *91*, 2749.
(9) Price, J. M.; Crofton, M. W.; Lee, Y. T. *J. Phys. Chem.* **1991**, *95*, 2182.
(10) Dopfer, O.; Olkhov, R. V.; Maier, J. P. *J. Phys. Chem. A* **1999**, *103*, 2982.
(11) Olkhov, R. V.; Nizkorodov, S. A.; Dopfer, O. *Chem. Phys.* **1998**, *239*, 393.
(12) Holmgren, S. L.; Waldman, M.; Klemperer, W. *J. Chem. Phys.* **1977**, *67*, 4414.
(13) Hutson, J. M.; Howard, B. J. *Mol. Phys.* **1980**, *41*, 1113.
(14) Light, J. C.; Bačić, Z. *J. Chem. Phys.* **1987**, *87*, 4008.
(15) Meuwly, M.; Bemish, R. J. *J. Chem. Phys.* **1997**, *106*, 8672.
(16) Roth, D.; Nizkorodov, S. A.; Maier, J. P.; Dopfer, O. *J. Chem. Phys.* **1998**, *109*, 3841.
(17) Frisch, M. J.; Trucks, G. W.; Schlegel, H. B.; Gill, P. M. W.; Johnson, B. G.; Robb, M. A.; Cheeseman, J. R.; Keith, T.; Petersson, G. A.; Montgomery, J. A.; Raghavachari, K.; Al-Laham, M. A.; Zakrzewski, V. G.; Ortiz, J. V.; Foresman, J. B.; Cioslowski, J.; Stefanov, B. B.; Nanayakkara, A.; Challacombe, M.; Peng, C. Y.; Ayala, P. Y.; Chen, W.; Wong, M. W.; Andres, J. L.; Replogle, E. S.; Gomperts, R.; Martin, R. L.; Fox, D. J.; Binkley, J. S.; Defrees, D. J.; Baker, J.; Stewart, J. P.; Head-

Gordon, M.; Gonzalez, C.; Pople, J. A. *Gaussian 94*, revision e.2; Gaussian, Inc.: Pittsburgh, PA, 1995.
(18) Woon, D. E.; Dunning, T. H., Jr. *J. Chem. Phys.* **1993**, *99*, 1914.
(19) Meuwly, M.; Maier, J. P.; Rosmus, P. *J. Chem. Phys.* **1998**, *109*, 3850.
(20) Boys, S. F.; Bernardi, F. *Mol. Phys.* **1970**, *19*, 553.
(21) Ho, T. S.; Rabitz, H. *J. Chem. Phys.* **1996**, *104*, 2584.
(22) Hutson, J. M. *BOUND Computer Program*, version 5; distributed by Collaborative Computational Project No. 6 of the UK Engineering and Physical Sciences Research Council, 1993.
(23) Johnson, B. R. *J. Comput. Phys.* **1973**, *13*, 445.
(24) Hutson, J. M. *Comput. Phys. Comm.* **1994**, *84*, 1.
(25) Rehfuss, B. D.; Jagod, M.-F.; Xu, L.-W.; Oka, T. *J. Mol. Spectrosc.* **1992**, *151*, 59.
(26) Schwenke, D. W.; Truhlar, D. G. *Comput. Phys. Commun.* **1984**, *34*, 57.
(27) Le Roy, R. J. *LEVEL Computer Program*; University of Waterloo Chemical physics report cp-330, 1992.
(28) Hutson, J. M.; Ashton, C. J. RESFIT Computer Program, 1982.
(29) Ashton, C. J.; Child, M. S.; Hutson, J. M. *J. Chem. Phys.* **1983**, *78*, 4025.
(30) Meuwly, M.; Hutson, J. M. *J. Chem. Phys.* **1999**, *110*, 8338.
(31) Aziz, R. A.; Slaman, M. J. *Chem. Phys.* **1989**, *130*, 187.
(32) Press, W. H.; Teukolsky, S. A.; Vetterling, W. T.; Flannery, B. P. *Numerical Recipies in Fortran*; Cambridge University Press: Cambridge, 1992.
(33) Meuwly, M. *J. Chem. Phys.* **1999**, *111*, 2633.
(34) Gutowsky, H. S.; Klots, T. D.; Chuang, C.; Schmuttenmaer, C. A.; Emilsson, T. *J. Chem. Phys.* **1987**, *86*, 569.
(35) McIlroy, A.; Lascola, R.; Lovejoy, C. M.; Nesbitt, D. J. *J. Chem. Phys.* **1991**, *95*, 2636.
(36) Liu, S.; Bačić, Z.; Moskowitz, J. W.; Schmidt, K. E. *J. Chem. Phys.* **1994**, *100*, 7166.
(37) Suhm, M. A.; Watts, R. O. *Phys. Rep.* **1991**, *204*, 293.
(38) Sandler, P.; oh Jung, J.; Szczesniak, M. M.; Buch, V. *J. Chem. Phys.* **1994**, *101*, 1378.
(39) Nizkorodov, S. A.; Meuwly, M.; Maier, J. P.; Dopfer, O.; Bieske, E. J. *J. Chem. Phys.* **1998**, *108*, 8964.
(40) Hutson, J. M. *J. Chem. Phys.* **1992**, *96*, 6752.
(41) Lewerenz, M. *J. Chem. Phys.* **1996**, *104*, 1028.
(42) Liu, S.; Bačić, Z.; Moskowitz, J. W.; Schmidt, K. E. *J. Chem. Phys.* **1994**, *101*, 10181.
(43) Lugez, C. L.; Jacox, M. E.; Johnson, R. D., III *J. Chem. Phys.* **1999**, *110*, 5037.